



Original Articles

Modeling thermal comfort in different condition of mind using satellite images: An Ordered Weighted Averaging approach and a case study

Naeim Mijani^a, Seyed Kazem Alavipanah^{a,*}, Saeid Hamzeh^a, Mohammad Karimi Firozjaei^a, Jamal Jokar Arsanjani^b

^a Department of GIS and Remote Sensing, Faculty of Geography, University of Tehran, Tehran, Iran

^b Geoinformatics Research Group, Department of Planning and Development, Aalborg University Copenhagen, A.C. Meyers Vænge 15, DK-2450 Copenhagen, Denmark



ARTICLE INFO

Keywords:

Thermal comfort
Remote sensing
MCDA
OWA
Quality of life
Tehran

ABSTRACT

One of the most important signs of decreasing quality of life in urban environments is the reduction of thermal comfort. Heat discomfort has a negative impact on physical and mental performance of humans. Hence, it is of outmost importance to monitor thermal comfort patterns in cities and study its effect on people. The main objective of this study is to present a spatial multi-criteria decision analysis (MCDA) model for modeling thermal comfort for Tehran as a case study. For doing so, the reflectance and thermal information extracted from Landsat-8 satellite images, ASTER digital elevation model, MOD07 water vapor, and meteorological/climatic datasets were used. Several indicators including the downward shortwave radiation (SWD) and longwave radiation (LWD) to surface, upward longwave radiation (LWU) from the surface, brightness, greenness and wetness of the surface were derived. An Ordered Weighted Averaging (OWA) method was adapted considering different mental circumstances e.g., extremely pessimistic, pessimistic, neutral, optimistic and extremely optimistic. Our findings determine the geographical variation of thermal comfort across our study area e.g., the cold periods of the year are spread in the west and north-west side and the warm periods of the year on the west and north-west, while the central, northern, and eastern regions have a more favorable thermal comfort than other regions. The areal percentage of very suitable thermal comfort category for very pessimistic, pessimistic, neutral, optimistic, and very optimistic during the warm period of the year was 2.7, 5.1, 4.4, 13.4 and 1.18, respectively and in the cold period of the year was 9.1, 13.3, 18.3, 28.9 and 33.9, respectively. In both warm and cold periods with increasing degree of optimism, the area of favorable thermal comfort classes increases, while the area of unfavorable thermal comfort categories decreases. Our results and conclusions drawn from our proposed approach are useful for urban planners and public health researcher for monitoring quality of life in cities.

1. Introduction

Nowadays, more than 55% of the world's population live in urban environments (Malik and Dewanker, 2018) and this rate is expected to reach 68% by 2050 (United Nations, 2018). The rise of urban population over the past decades has caused the physical expansion of cities. On the other hand, physical development of cities has made a lot of changes in terms of land use, morphology, and urban heat island (Weng et al., 2018; Karimi Firozjaei and Kiavarz, 2018; Huang et al., 2018; Yan et al., 2018) as a result of social and environmental abnormalities (Mirbagheri and Alimohammadi, 2017).

Replacing natural land cover with impervious surfaces such as pavements, buildings, and other urban structures can change the absorption of

downward shortwave radiation (SWD) and longwave radiation (LWD) to surface, temperature, humidity, wind patterns, and the reduction of surface cooling effects caused by evapotranspiration (Musse et al., 2018; Wang et al., 2018a). In addition, the heat and pollution caused by vehicles, industries, and other anthropogenic activities increase the pollution and air temperature of urban areas (Santamouris and Kolokotsa, 2015). These widespread anthropogenic changes have negative consequences such as environmental degradation, which ultimately leads to a decline in quality of life (Musse et al., 2018).

One of the most important signs of decreasing the quality of life in urban environments is the reduction of human thermal comfort (Shek and Chan, 2008; Zhu et al., 2018; Geletič et al., 2018). The rapid growth of cities and the expansion of urban areas have led to major

* Corresponding author.

E-mail addresses: Naeim.mijani@ut.ac.ir (N. Mijani), salavipa@ut.ac.ir (S.K. Alavipanah), saeid.hamzeh@ut.ac.ir (S. Hamzeh), mohammad.karimi.f@ut.ac.ir (M.K. Firozjaei), jja@plan.aau.dk (J.J. Arsanjani).

<https://doi.org/10.1016/j.ecolind.2019.04.069>

Received 3 February 2019; Received in revised form 4 April 2019; Accepted 24 April 2019

1470-160X/ © 2019 Published by Elsevier Ltd.

environmental changes and change in thermal comfort conditions, especially in urban open spaces. Thermal comfort is a condition of mind that expresses the satisfaction of the surrounding thermal environment (Choi and Yeom, 2019; Li et al., 2018). Heat discomfort has a negative effect on human physical and mental performance, including fatigue, sleep disturbances, reduced ability to perform mental activities, health problems and even death (García-Herrera et al., 2010; Xu et al., 2012; Wang et al., 2018b). Therefore, monitoring, prediction, and recognition of thermal comfort patterns is very important for solving human health challenges as well as planning physical sights, social and economic services, and energy consumption in cities (Bhattacharjee and Ghosh, 2015; Mushore et al., 2018).

The thermal comfort in urban environments is caused by the interactions of climatic conditions, surface biophysical characteristics and structural characteristics of urban areas. The heterogeneity in the climatic conditions of urban areas and the characteristics of urban surfaces causes spatial heterogeneity of citizens' thermal comfort (Mushore et al., 2018). According to (Wang et al., 2004; Stathopoulou et al., 2005; Sobrino et al., 2013; Xu et al., 2017; Mushore et al., 2018; Song and Wu, 2018), thermal comfort in urban environments is mainly affected to environmental and surface conditions, including SWD and LWU to surface, LWU from the surface, brightness, greenness and wetness of the surface (Tsunematsu et al., 2016).

In previous studies, the thermal comfort of a city was calculated based on the climatic data of one or more meteorological stations (Toy et al., 2007; Kántor and Unger, 2010; Gómez et al., 2013; Van Hove et al., 2015; Qaid et al., 2016; Katavoutas et al., 2016; Morris et al., 2017). The data recorded at the synoptic stations lacks a sufficient spatial resolution and therefore, is not possible to accurately model the thermal comfort at a local scale based on local measurements across the entire city (Liu et al., 2018). Because, a few climatological measurements across the entire city instead of a continuous measurement are inserted in the model. This is why remote sensing data should be used to gain a continuous measurement for each pixel in the city.

Furthermore, it can provide additional data products that can be easily integrated with geographical information systems (GIS) (Zawadzki et al., 2005). Over the past years, it has become possible to use space-based measurements in order to study the intensity and spatial distribution of thermal discomfort in urban environments and several studies including (Wang et al., 2004; Stathopoulou et al., 2005; Sobrino et al., 2013; Xu et al., 2017; Song and Wu, 2018; Mahmoud and Gan, 2018) have acknowledged the advantages of doing so. However, the models presented in these studies for modeling thermal comfort are limited to regression analysis (Wang et al., 2004; Stathopoulou et al., 2005; Sobrino et al., 2013; Xu et al., 2017; Mushore et al., 2018; Song and Wu, 2018) and offer low flexibility to consider the condition of mind of each group of individuals.

In many cases, environmental decision-making in the risk space is affected by the level of risk-taking and risk-averse decision-making. Both theoretical and empirical evidences show that decision makers with optimistic (or risk-taking) attitudes tend to be more concerned with the desirable properties (better values) of alternatives, while pessimistic (or risk-averse) decision makers tend to concentrate more on the undesirable properties (worse values) of alternatives (Firozjahi et al., 2018b). The literature lacks of considering the concept of risk in decision-making to generate a thermal comfort map. The OWA decision-making model has the potential to incorporate the concept of risk into multi-criteria decision making (Malczewski, 2006). The process of making a final decision in this method is based on risk-taking and risk-averse of the decision maker.

Generally, thermal comfort varies for different individuals, therefore, individuals have different mental circumstances of thermal comfort based on various parameters such as age, weight, health status and degree of sensitivity to thermal waves. For this reason, each location due to its climatic conditions, geometric and biophysical structure of its surface might offer a suitable thermal comfort for a particular group of

individuals, while it might be unsuitable for other groups. For example, to select suitable locations of thermal comfort for sensitive and high-risk groups e.g., elderly people, children and heat sensitive individuals, pessimistic condition of mind should be considered. In this case, suitable regions are identified based on a set of rules i.e., whether the region is suitable in terms of thermal comfort. On the other hand, for those individuals, who are less or insensitive to thermal conditions, an optimistic condition of mind should be considered.

Hence, the main objective of this study is to propose an approach based on a spatial multi-criteria decision analysis (MCDA) model for modeling thermal comfort in different scenarios. To do so, the OWA model was used for a case study of Tehran in the warm and cold periods of the year in extremely pessimistic, pessimistic, neutral, optimistic and extremely optimistic scenarios. The contribution of the present study is (a) the modeling of thermal comfort using a MCDA model based on the set of environmental and biophysical parameters of the surface; and (b) the consideration of different scenarios in modeling thermal comfort.

The remainder of this paper is structured as follows. Section 2 presents the study area and introduces the data and methods used in the study. Section 3 presents the results, while Section 3 discusses the findings, and finally the paper concludes some remarks and suggestions for future works in Section 5.

2. Materials and methods

2.1. Study area

The chosen study area is Tehran, the capital of Iran. Tehran is the largest and the most important city in Iran, which is spread from 51° 17' to 51° 33' eastern and 35° 36' to 35° 45' northern. It is located in the north of Iran in the southern slope of the Alborz Mountain and the northern edge of the central desert of Iran, which offers a heterogeneous weather condition across the city. The current population of Tehran with a growth rate of 1.31% (in 2018) is 8,895,947, and is projected to reach 10,664,297 in 2035 (United Nations, 2018; world-populationreview, 2018). The pressure of the population and the demand for housing has led to the conversion of farms and open areas to residential areas and even construction on the top of the surrounding hills. The city has a relatively irregular urban pattern and a heterogeneous distribution of green spaces with a per capita green space of 4.5 m² per person, which is substantially below the global average at about 20–25 m² per person. The geographic location of the study area is shown in Fig. 1.

2.2. Data

The data used in this study as well as their description is shown in Table 1.

Meteorological and climatic data measured at 6 synoptic stations located in the study area, including air temperature and relative humidity were used. Meteorological and synoptic stations are spread across diverse locations of the city reflecting heterogeneous topography. The synoptic stations characteristics is shown in the Table 2.

2.3. Methodology

2.3.1. A conceptual model for modeling thermal comfort

The proposed approach for modeling thermal comfort is shown in Fig. 2.

2.3.2. The OWA operator

The OWA, introduced by Yager (1988), is a multi-criteria aggregation operator, which has been widely used in a broad range of spatial decision making and assessment applications (Malczewski and Rinner, 2015). The OWA operator aggregates the standardized factors using two sets of weights: the factor weights (w_1, w_2, \dots, w_n), and the order

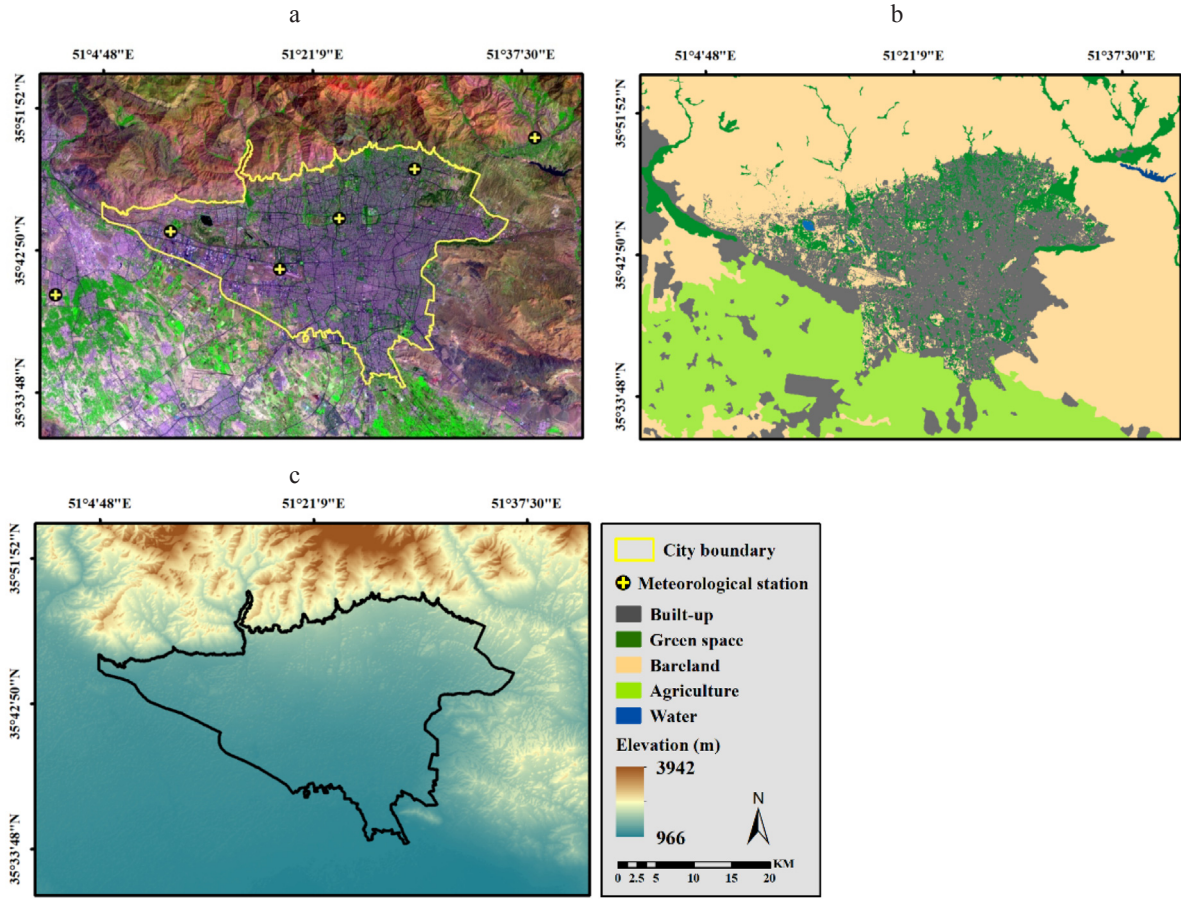


Fig. 1. (a) A true color composite of Landsat reflective bands, (b) major land cover types, (c) the Digital Elevation Model.

weights ($\lambda_1, \lambda_2, \dots, \lambda_n$). Given a set of standardized factors ($a_{i1}, a_{i2}, \dots, a_{in}$) for the i th pixel ($i = 1, 2, \dots, m$), the OWA operator is described below (Yager, 1988):

$$V(A_i) = \sum_{j=1}^n \frac{\lambda_j U_{ik} Z_{ik}}{\sum_{k=1}^n \lambda_k U_k} \quad (1)$$

$\sum_{j=1}^n \lambda_j = 1$ and $0 < \lambda_k < 1$

$V(A_i)$ represents the overall score of the i th pixel and $Z_{i1} \geq Z_{i2} \geq \dots \geq Z_{in}$ is the sequence generated by ordering the standardized factor values of the i th pixel. U_k is the weight of the k th factor, which is measured from the ordered values of the factors (Z_{ik}). The reordering process controls the OWA function, which involves linking the order weight of λ_k with a particular ordered factor value (Z_{ik}) in the i th pixel. The first order weight, λ_1 , is associated with the highest factor value for the i th pixel, the second order weight, λ_2 , is associated to the second highest value for the same pixel, and finally λ_n is associated to the lowest factor value (Jelokhani-Niaraki and Malczewski, 2015; Firozjaei et al., 2018b).

The basic principle of the OWA is the possibility to implement a variety of combination operators by selecting different set of order weights (Jelokhani-Niaraki and Malczewski, 2015; Firozjaei et al., 2018b). For example, the OWA operator serves as Boolean Intersection (AND), Weighted Linear Combination (WLC), and Boolean Union (OR) map combination rules when the set of order weights are (0, 0, ..., 1), (n-1, n-1, ..., n-1), and (1, 0, ..., 0), respectively. The set of order weights implicitly control the degree of risk (or ORness degree) in the decision-making process. The ORness or risk-taking degree shows the location of OWA operator from AND (minimum or very pessimistic

decision strategy) to OR (maximum or very optimistic decision strategy) values. In other words, it shows the risk-taking or risk-aversion tendency of a decision-maker. The greater and lower values of ORness put emphasis on the higher values and the lower values in a set of the factors associated with the i th pixel, respectively (Jelokhani-Niaraki and Malczewski, 2015). The degree of ORness can be related to order weights through the following equation:

$$ORness = \sum_{k=1}^n \left(\frac{n-j}{n-1} \right) \lambda_k \quad 0 \leq ORness \leq 1 \quad (2)$$

The relation between ORness values and decision-making conditions of mind strategies in the OWA model is shown in Fig. 3.

Fig. 4 shows an example of the OWA operator for ORness = 0.25. For a set of standardized attribute values at the i th location, $a_{ij} = [0.4, 0.9, 0.5]$, the procedure involves the following steps:

- (i) identifying the attribute weights according to $w_j = [0.2, 0.3, 0.5]$,
- (ii) ranking the attribute values and $z_{ij} = [0.9, 0.5, 0.4]$,
- (iii) re-ordering the attribute weights according to z_{ij} ; the attribute weights, $u_j = [0.3, 0.5, 0.2]$,
- (iv) calculating the order weights, $v_j = [0.027, 0.485, 0.488]$, and
- (v) calculating the OWA score for the location i ; $OWA_i = 0.462$.

2.3.3. Data preprocessing

Before computing and extracting various parameters such as spectral energy of reflective and thermal bands, it is necessary to collect LSE, LST, albedo, and surface biophysical characteristics, radiometric and atmospheric corrections of various bands from the input satellite images. Fast Line-of-sight Atmospheric Analysis of Hypercubes (FLAASH) algorithm was employed for atmosphere correction (Cooley

Table 1
The data used in this study.

Data type	Sources	Resolution (m)	Period	Description
Satellite image	Landsat 8 (OLI/TIRS)	30/100 m	2013–2018	Landsat 8 satellite imagery from path-row 164/035 was used for modeling surface biophysical characteristics such as land surface temperature (LST), Albedo, brightness, greenness, and wetness.
Digital elevation model	Advanced Spaceborne Thermal Emission and Reflection Radiometer (ASTER)	30		Global Digital Elevation Model (GDEM) of the study region with a spatial resolution of 30 m was used for modeling environmental parameters such as incoming radiation on the surface and Environmental Lapse Rate (ELR) effect.
MOD07 water vapor	Moderate Resolution Imaging Spectroradiometer (MODIS)	5000		The MODIS Atmospheric Profile product i.e., MYD07_12, contains the following features: (1) total ozone; (2) atmospheric stability; (3) temperature and moisture profiles; (4) and atmospheric water vapor. The MODIS atmospheric water–vapor product is an estimated total tropospheric column water vapor made from integrated MODIS infrared retrievals of atmospheric moisture profiles in clear scenes. This product was used for calculation of LST.
Air temperature	Meteorological stations	-		These datasets were used to calculate thermal comfort for the geographic location of each station at the time of satellite passage.
Relative humidity		-		

Table 2
The synoptic stations characteristics.

Station name	Longitude (°)	Latitude (°)	Elevation (m)
Shemiran	51.48	35.79	1549.12
Tehran (Mehrabad Airport)	51.31	35.69	1191.11
Lavasan	51.64	35.83	1863.23
Chitgar	51.17	35.73	1305.24
Shahriyar	51.02	35.67	1162.91
Geophysic	51.39	35.75	1418.63

et al., 2002) considering the importance of radiometric and atmospheric effects on LST. This module is based on MODTRAN 4 model, which inputs the time of satellite’s passage, the geographical position of the study area, the sensor’s elevation, solar radiation angle, and the atmospheric model of the region (Cooley et al., 2002; Weng et al., 2019). The collected data from the USGS included the Landsat Level-1 Precision Terrain (L1TP) data, which is suitable for time-series analysis. The geo-registration task was carried out resulting in an RMSE of < 12 m (Moghaddam et al., 2018; Weng et al., 2019). Thermal Infrared Sensor (TIRS) bands of Landsat 8 are acquired at 100 m resolution and then resampled to 30 m for compatibility with the other bands. The image-to-image geometric correction was conducted to match Landsat 8 image and GDEM.

2.3.4. Relevant parameters to thermal comfort

A literature review shows that heterogeneity in the characteristics of urban surfaces causes spatial heterogeneity of the thermal comfort of individuals in different urban areas mainly affected by environmental and surface conditions (Zhang et al., 2009). According to (De Ridder et al., 2004), vegetation cover and green space can reduce thermal stress and improve the environment and reduce contamination level and help to provide a better environment. Vegetation creates a natural air conditioning system by absorbing solar energy and transpiration of water through its leaves. Natural surfaces contain more moist than built-up in urban environments. Water, due to its high heat capacity, absorbs heat from its surroundings and maintains it, therefore moist reduces the surface temperature as well as the adjacent areas. Surface temperature of impervious surfaces, sidewalks and street level can become very high and subsequently increase the air temperature. When surface’s temperature rises, the radiation of the diffused and reflected sun increases, which increases the thermal comfort index. This means that the earth’s surface exposed to direct sun radiation receives and emits solar radiation resulting in increasing surface temperature, which impacts outdoor thermal comfort. Built-up, vegetation cover, and water body are three main land cover types in living environments, which play a big role in humans’ living environment and humans’ thermal sensation. Therefore, the relation between thermal comfort and built-up, vegetation cover and water body has to be further investigated. In the present study, six criteria representing environmental and biophysical of the surface including SWD and LWD to surface, LWU from the surface, Brightness, Greenness and Wetness of the surface have been considered for modeling thermal comfort.

2.3.4.1. Calculation of upward longwave radiation (LWU) from surface. The LWU is the thermal radiation flux, which is emitted from the earth’s surface to the atmosphere ($W m^{-2}$) and is measured by means of Stefan-Boltzmann model as Eq. (3) (Waters et al., 2002):

$$R_{L\uparrow} = \varepsilon_0 \times \sigma \times T_s^4 \tag{3}$$

where $R_{L\uparrow}$ is upward longwave radiation (LWU) from surface, ε_0 the emissivity coefficient, σ the Stefan-Boltzmann constant ($5.67 \times 10^{-8} W m^{-2} K^{-4}$), and T_s the LST (Kelvin). In this study, LST was calculated using split window (SW) algorithms (Weng et al., 2019). The normalized difference vegetation index (NDVI) base method is also applied to calculate the emissivity (Li et al., 2016; Panah et al., 2017;

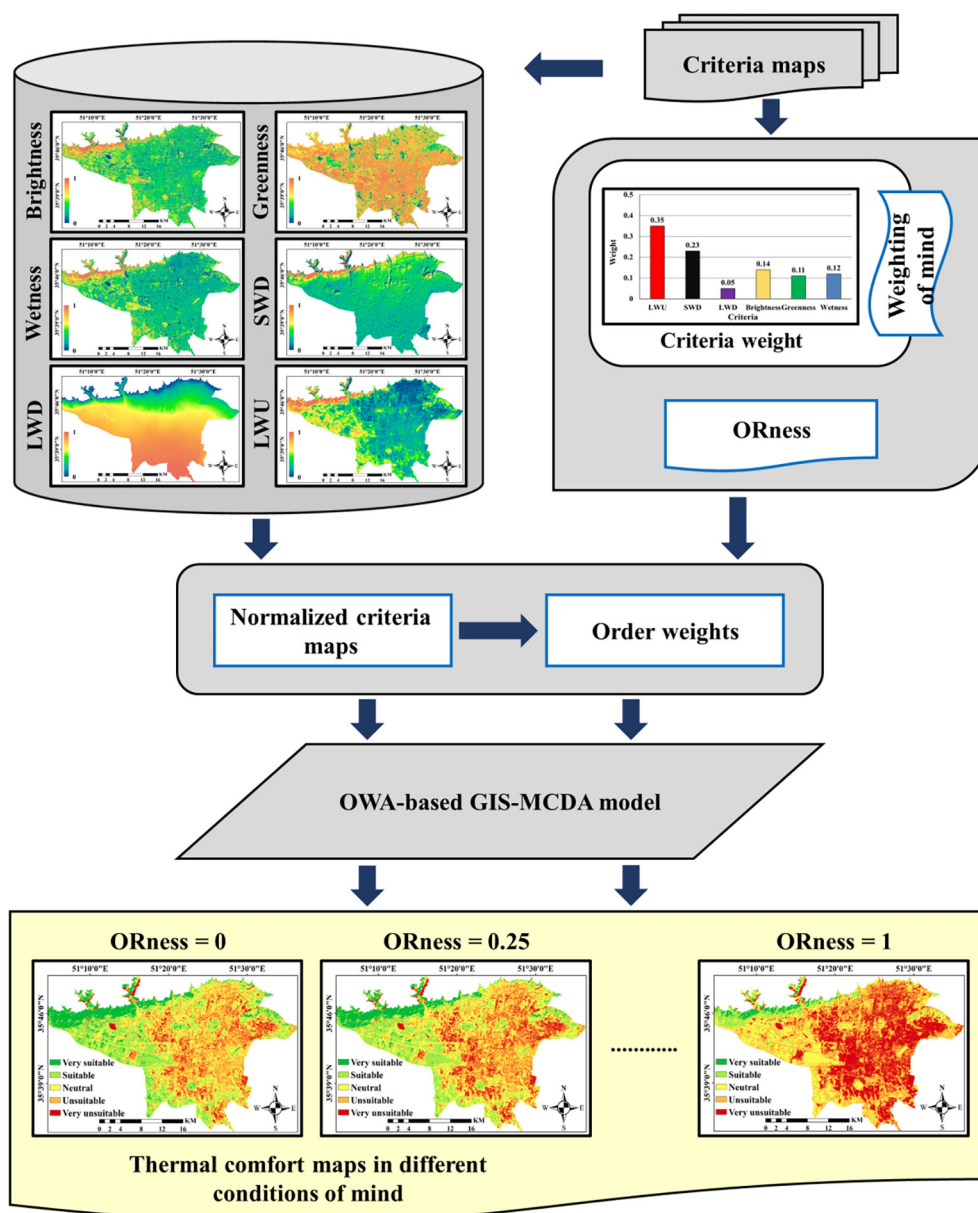


Fig. 2. The conceptual model for modeling thermal comfort.

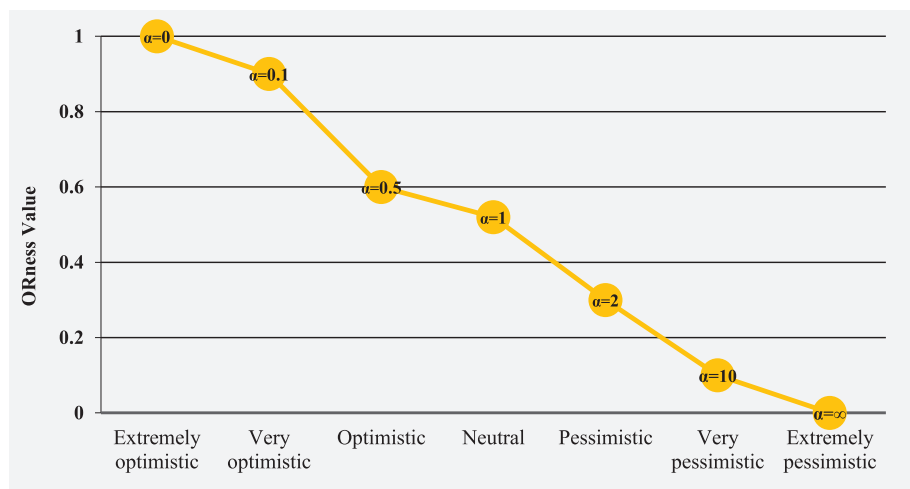


Fig. 3. The relation between ORness values and decision-making conditions of mind strategies (Kiavaz and Jelokhani-Niaraki, 2017).

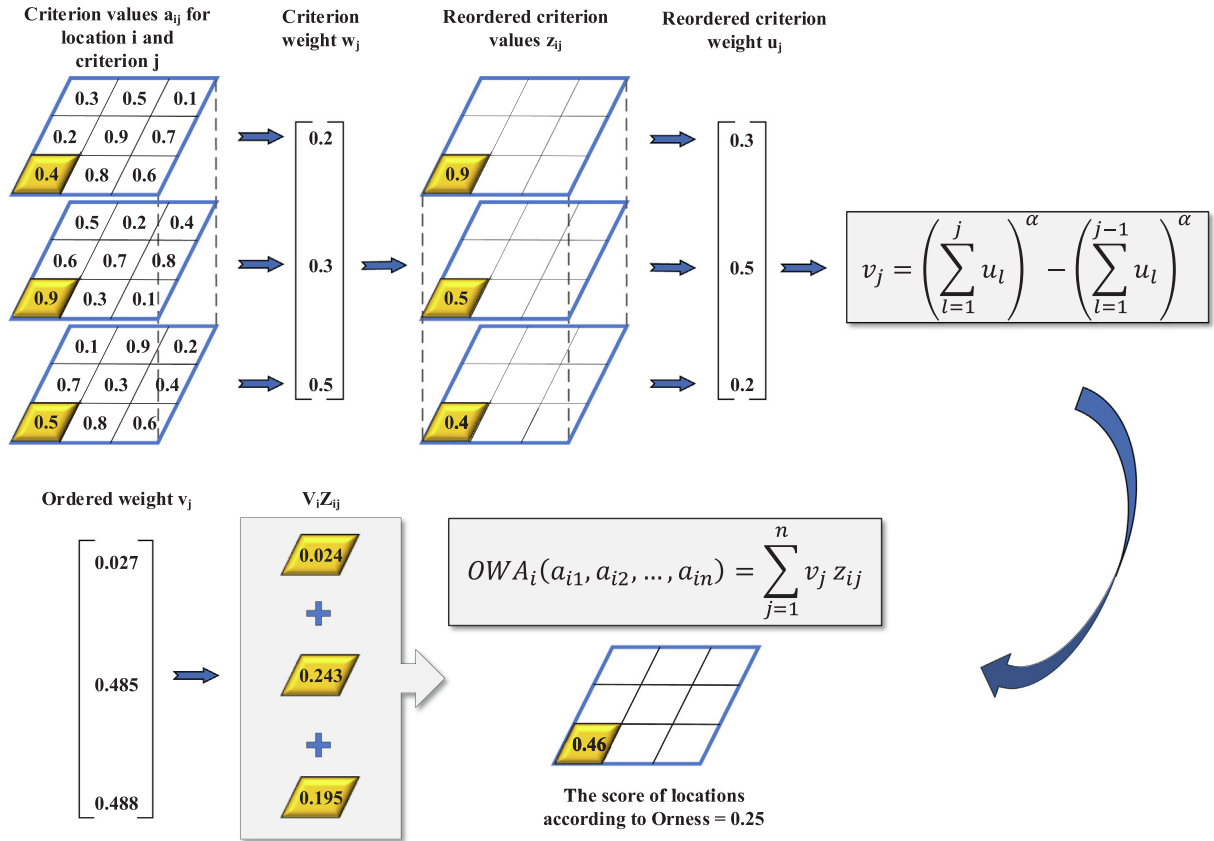


Fig. 4. An exemplary computation of the OWA for the i th location and $ORness = 0.25$.

Firozjaei et al., 2018a). In order to calculate LST through SW method, the amount of water vapor in the atmosphere is required. Hence, MOD07 product at 5 km resolution was used to estimate the amount of water vapor in the atmosphere.

2.3.4.2. Calculation of downward shortwave radiation (SWD) to surface. The amount of SWD to surface includes direct and diffuse solar radiation and direct and diffused reflected radiation from neighboring regions (Karimi Firozjaei et al., 2018; Weng et al., 2019). The value of this parameter depends on a set of criteria, such as topographic conditions of the surface, sky cloudiness, atmospheric conditions, temporal situation, latitude and longitude, albedo, and surface topographic conditions (Firozjaei et al., 2018b; Karimi Firozjaei et al., 2018). Given clear sky conditions, SWD to surface is measured as a constant using Eq. (4) (Waters et al., 2002):

$$R_{s_l} = G_{sc} \times \cos(\theta) \times d_r \times \tau_{sw} \quad (4)$$

where R_{s_l} is downward shortwave radiation to surface, G_{sc} the solar constant (1367 W m^{-2}); d_r the inverse squared relative distance of earth to sun, and τ_{sw} the atmospheric transmissivity.

The solar local incidence angle was calculated using Eq. (5) (Firozjaei et al., 2019; Duffie and Beckman, 2013).

$$\begin{aligned} \cos(\theta) = & \sin(\delta)\sin(\varphi)\cos(s) - \sin(\delta)\cos(\varphi)\sin(s)\cos(\gamma) \\ & + \cos(\delta)\cos(\varphi)\cos(s)\cos(w) + \cos(\delta)\sin(\varphi)\sin(s)\cos(\gamma)\cos(w) \\ & + \cos(\delta)\sin(\gamma)\sin(s)\sin(w) \end{aligned} \quad (5)$$

where δ is the declination of earth, φ the latitude of the pixel, s the slope, γ the surface aspect angle, and w the hour angle, all in radian.

2.3.4.3. Calculation of downward longwave radiation (LWD) to surface. The LWD is the downward thermal radiation flux from the atmosphere (W m^{-2}), which is calculated from the Stefan-Boltzmann

model as presented in Eq. (6):

$$RL_l = \epsilon_a \sigma T_a^4 \quad (6)$$

where RL_l is downward longwave radiation to the surface, ϵ_a is the atmospheric emissivity coefficient, σ Stefan-Boltzmann's constant, and T_a is the air temperature of the near land surface (Kelvin) (Allen et al., 2002). In this study, for modeling air temperature for each day, GDEM and the recorded air temperature in the meteorological stations were used based on the environmental lapse rate (ELR).

2.3.4.4. Modeling the biophysical characteristics. One of the widely used methods for describing land surface is to calculate Tasseled Cap Transformation (TCT) compounds. The TCT compounds represent information such as brightness, greenness, and wetness. (Liu et al., 2014; Liu et al., 2015; Karimi Firozjaei and Kiavarz, 2018). Greenness in urban environments such as parks, trees, grasses, roof top vegetation reduces cities' temperature through evapotranspiration, reflectance, and blocking the solar radiation winds. Brightness indicates impervious surfaces and bare lands. Greenness represents vegetation coverage and wetness indicates the wetness on top of the surface. Wetness indicates water and moist on the surface, which has a cooling effect.

Various studies have been carried out on the development of TCT bands combinations for satellite imagery related to different sensors (Liu et al., 2014). In this study, Landsat 8 reflective bands were used to calculate surface biophysical properties. The coefficients related to TCT indicators for Landsat 8 images are shown in Table 3 (Liu et al., 2014; Baig et al., 2014; Karimi Firozjaei and Kiavarz, 2018).

2.3.5. Standardization of criteria maps

The OWA-based GIS-MCDA requires the criteria values to be standardized, which means projecting them into the same value scale while expressing the same meaning. For instance, high values represent

Table 3

The coefficients used for calculation of TCT indicators for Landsat-8 images.

Component	Band 1	Band 2	Band 3	Band 4	Band 5	Band 6	Band 7
Brightness	–	0.3029	0.2786	0.4733	0.5599	0.508	0.1872
Greenness	–	–0.2941	–0.243	–0.5424	0.7276	0.0713	–0.1608
Wetness	–	0.1511	0.1973	0.3283	0.3407	–0.7117	–0.4559

favorite areas and low values represent least favorite areas. The standardization was carried out using minimum and maximum values of each criterion. Eqs. (7) and (8) can respectively be used to standardize criteria maps.

$$amax_{ij} = \frac{S_{ij} - S_j^{min}}{S_j^{max} - S_j^{min}} \quad (7)$$

$$amin_{ij} = \frac{S_j^{max} - S_{ij}}{S_j^{max} - S_j^{min}} \quad (8)$$

where $amax_{ij}$ is standardized values of maximized criterion, $amin_{ij}$ standardized values of minimized criterion, S_{ij} the raw value for the i th location and the j th criterion, S_j^{min} represents the minimum value for the j th criterion, S_j^{max} is the maximum value for the j th criterion, a_{ij} is the standardized value for the i th location and the j th criterion. The standardized maps range from 0 to 1 (Firozjaei et al., 2018b). The effect of different criteria on the thermal comfort of the environment varies over the warm and cold period of the year. For example, although vegetation cover is favorable in warm season and it has a positive effect, but often shows negative effects in cold seasons (Thom, 1959). Generally, during the warm period, the most amount of vegetation cover and surface wetness, and the least amount of SWD and LWD to surface, LWU from the surface, surface Brightness are important for favorable thermal comfort conditions. But for the cold period of the year, in order to provide suitable thermal comfort conditions, the maximum amount of SWD and LWD to surface, LWU from the surface, surface Brightness, and the least amount of vegetation cover and surface wetness criteria are important.

2.3.6. Weighting effective criteria

In this study, for weighing the effective criteria on thermal comfort the objective weighting has been used. According to the correlation coefficient of the values of each of the effective criteria with the thermal comfort index values in the geographic location of the meteorological stations for the period of 2013–2018, the weight of each criterion is calculate using Eq. (9).

$$W_i = \frac{R_i^2}{\sum_{i=1}^n R_i^2} \quad (9)$$

where W_i is the weight of the i th criterion, R_i^2 the correlation coefficient of the i th criterion values with thermal comfort index values, and n the number of criteria. Accordingly, a criterion that has a higher correlation coefficient with thermal comfort index has more impact on it and should have a higher weight in the MCDA.

2.3.7. Thermal comfort at the meteorological stations

In this study, using the relative humidity and air temperature values recorded at meteorological stations, thermal comfort is calculated for the geographic location of each station at the time of satellite passage based on the Eq. (10).

$$DI = T - 0.55(1 - 0.01RH)(T - 14.5) \quad (10)$$

where DI is the thermal comfort indicator, T temperature ($^{\circ}\text{C}$) and RH relative humidity (%) in the geographic location of the ground stations and meteorological stations. The Discomfort Index (DI) was first introduced by Thom (1959), which, as a linear equation, determines the thermal comfort of the human in the open space based on the

temperature and relative humidity. The DI index describes the relationship between the living environment and human's thermal sensation (Carlucci and Pagliano, 2012). In previous studies, the features of the living environment are rarely examined. The study by (Xu et al., 2017) shows that human's perception of thermal discomfort is also spatial and varies as we move across space. Based on the conceptual model presented in Fig. 2, thermal comfort maps for the study area were prepared for ORness values 0, 0.25, 0.5, 0.75 and 1, corresponding to extremely pessimistic (ORness = 0), pessimistic (ORness = 0.25), neutral (ORness = 0.5), optimistic (ORness = 0.75) and extremely optimistic (ORness = 1) condition of mind in modeling thermal comfort.

3. Results

In this study, six criteria reflecting environmental and surface biophysical characteristics including SWD and LWD to surface, LWU from the surface, brightness, greenness and wetness of the surface were considered. Each of the criteria was standardized based on its range of values. Criteria maps of environmental parameters and surface biophysical characteristics of the effective on thermal comfort for the periods related to the warm and cold period of the year are shown in Fig. 5.

SWD and LWD to the surface, LWU from the surface, built-up lands, vegetation cover and water body play divergent roles on DI . Hence, these parameters were extracted for the same geographic location of the meteorological stations. Also, their DI values were calculated based on air temperature and relative humidity. To survey the effect of each of the environmental parameters and surface biophysical characteristics on the thermal comfort index, the correlation coefficient between each of parameter and the thermal comfort indicator is calculated. The results related to the effect of each of the environmental parameters and surface biophysical characteristics on the thermal comfort index are shown in Table 4.

The results presented in Table 4 show the effect of each of the environmental parameters and surface biophysical characteristics on thermal comfort index. SWD and LWD to surface, LWU from surface parameters with correlation coefficients 0.56, 0.21, and 0.84, respectively, while the surface biophysical characteristics of brightness, greenness and wetness with correlation coefficients 0.38, 0.28 and 0.30 respectively had the highest effect on the thermal comfort index DI . Based on the correlation coefficient between each of the environmental parameters and surface biophysical characteristics with the values of DI 's thermal comfort index in the geographic location of the meteorological stations, the weight of each of the criteria shown in Fig. 6 is calculated in the MCDA model. The weight of each of the effective criteria on the thermal comfort of the study area is shown in Table 5.

The classified maps of thermal comfort in the condition of mind of the warm and cold periods of the year are shown in Fig. 6.

Fig. 6 shows that in the cold period of the year, the west and north-west parts, and in the warm period of the year, the central, northern, and eastern parts offer suitable and very suitable thermal comfort than the remaining parts of the study area. In different condition of mind, the area and spatial distribution of different classes of thermal comfort are different. The area of thermal comfort classes is calculated for warm and cold periods of the year for different condition of mind and is shown in Fig. 7.

According to Fig. 7, in both warm and cold periods with increasing

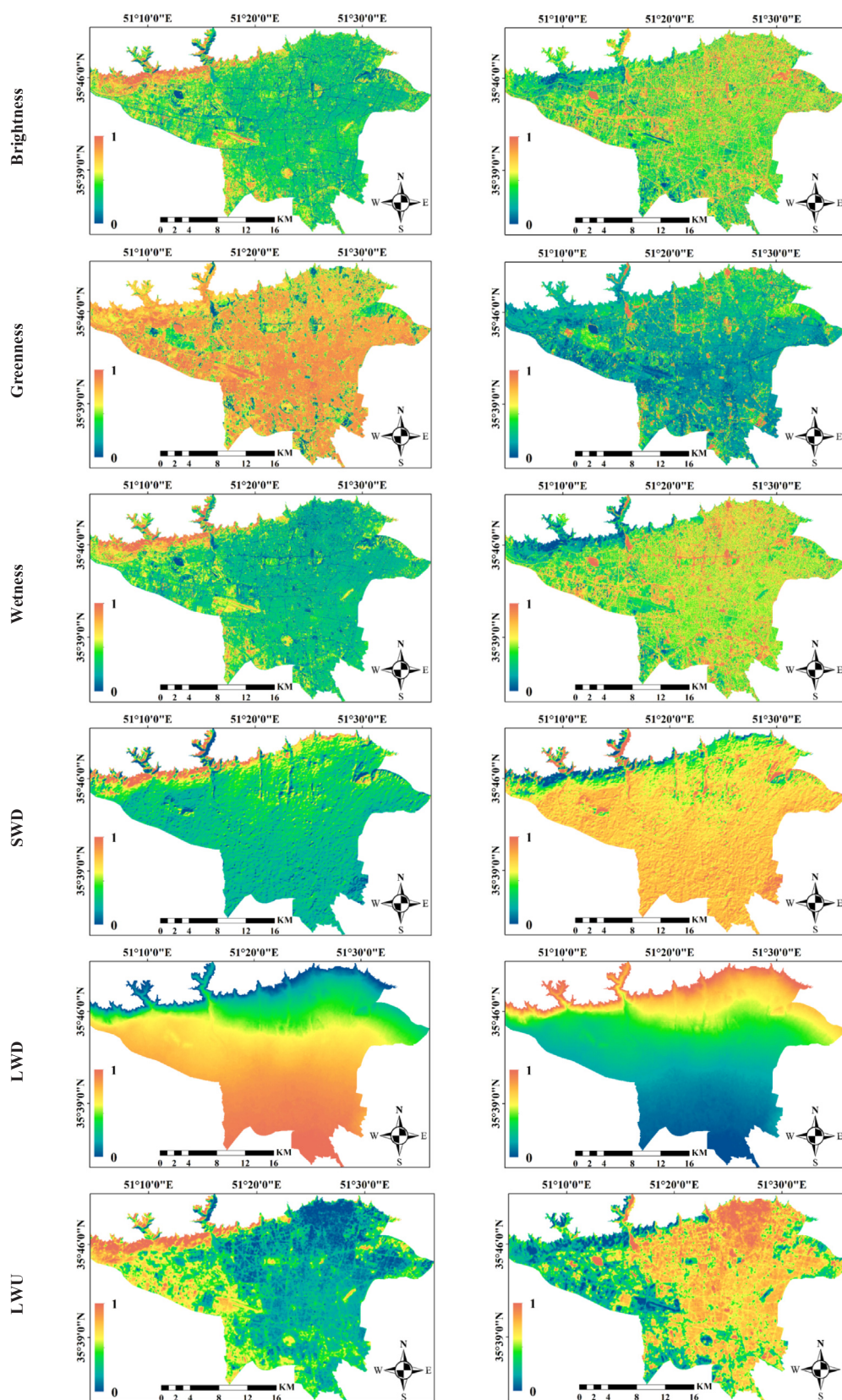


Fig. 5. Criteria maps of environmental parameters and surface biophysical characteristics for the warm and cold periods of the year.

degree of optimism, the area of suitable and the very suitable classes of thermal comfort increased. Also, the area of unsuitable and very unsuitable classes of thermal comfort decreased so that the areal

percentage for category of very suitable for extremely pessimistic, pessimistic, neutral, optimistic and extremely optimistic condition of mind during the warm period of the year, is 2.7, 1.5, 8.4, 13.4 and 13.1,

Table 4
The correlation between discomfort index and each environmental parameter and surface biophysical characteristics.

Selected criteria	LWU	SWD	LWD	Brightness	Greenness	Wetness
R ²	0.8456	0.5627	0.2173	0.3824	0.2817	0.3037

Table 5
The weights of criteria on the thermal comfort of the study area in the MCDA model.

Selected criteria	LWU	SWD	LWD	Brightness	Greenness	Wetness
Weight	0.35	0.23	0.05	0.14	0.11	0.12

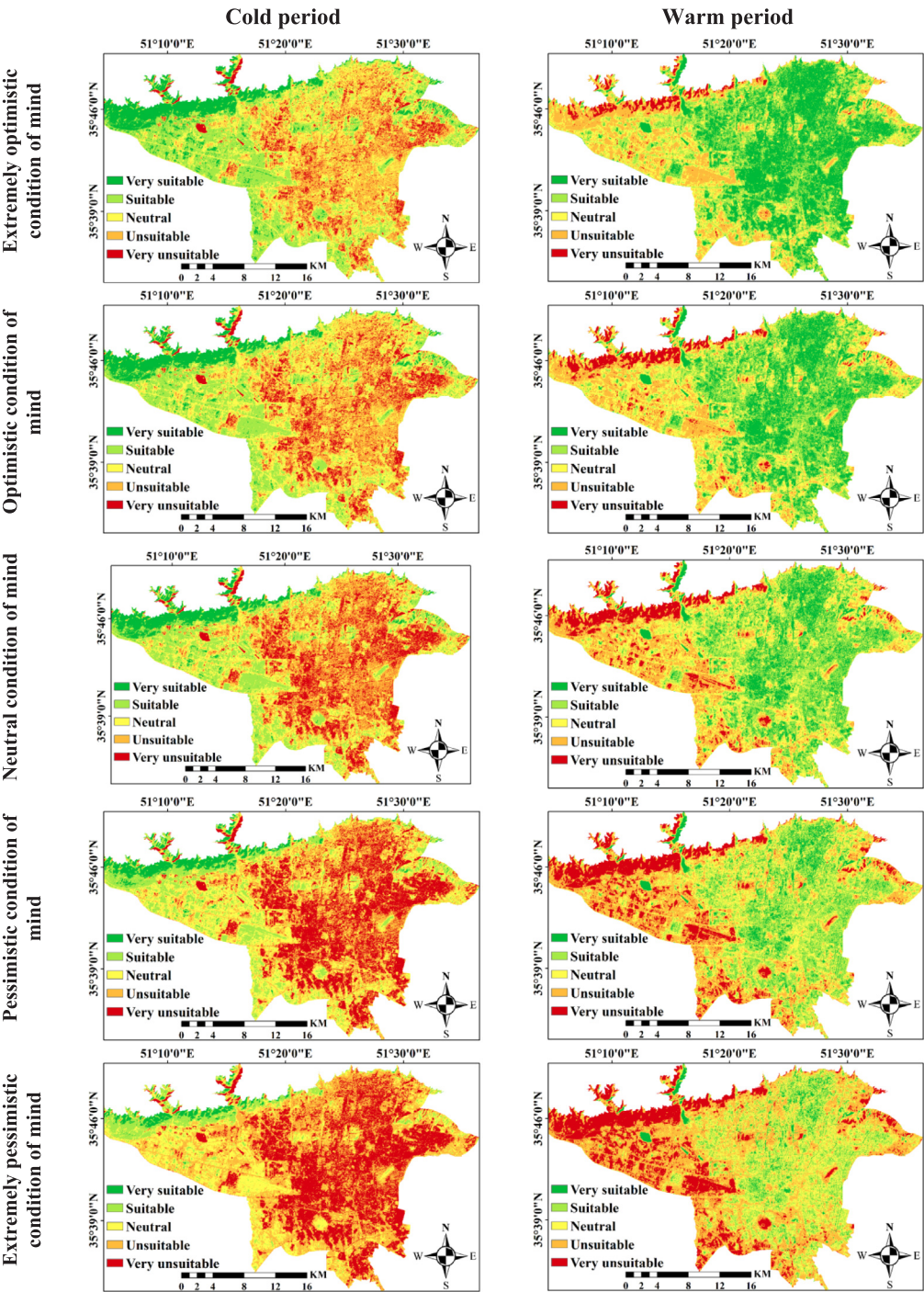


Fig. 6. The classified maps of thermal comfort in condition of mind for the warm and cold periods.

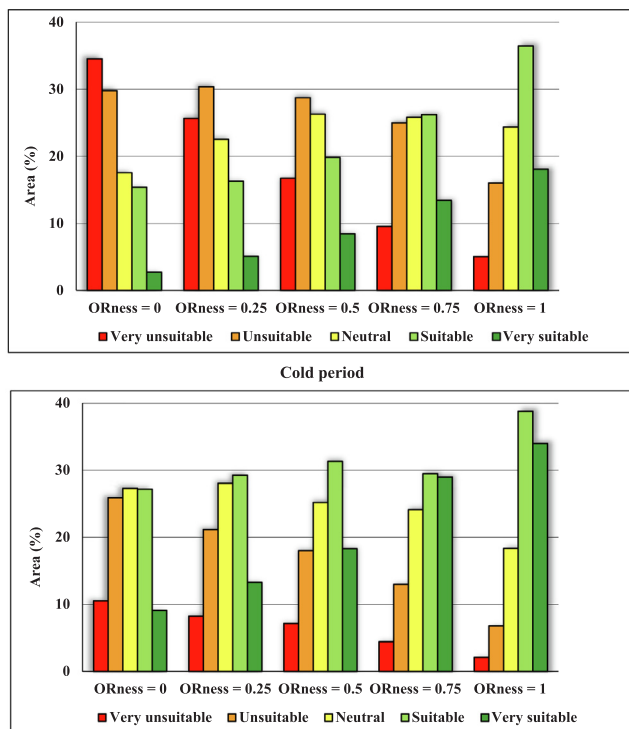


Fig. 7. The area of thermal comfort classes in the warm and cold periods of the year for different condition of mind.

respectively, and in the cold period, is 9.1, 13.3, 18.3, 28.9 and 33.9, respectively.

4. Discussions

The thermal comfort of a city is usually calculated based on climatic data collected at meteorological stations (Van Hove et al., 2015; Toy et al., 2007; Qaid et al., 2016; Kántor and Unger, 2010; Morris et al., 2017; Gómez et al., 2013; Geletič et al., 2018). The data recorded at synoptic stations lack a fine spatial resolution. Due to this lack as well as the heterogeneity of urban environments, measurements from a few synoptic stations' result in uncertainties in calculated thermal comfort patterns across the entire city. Hence, the continuous spatial coverage and concurrency of remote sensing data as well as provision of energy reflectance and thermal information allow us to obtain more accurate results. On the other hand, previous remote sensing-based models are limited to statistical relationships and regressions (Mushore et al., 2018; Song and Wu, 2018; Xu et al., 2017; Stathopoulou et al., 2005; Wang et al., 2004; Sobrino et al., 2013), which makes them less flexible to consider the condition of mind of individuals. The OWA model has been used in various fields such as land use modelling (Malczewski, 2006), health analysis (Clements et al., 2006), tourism planning (Claus and Martin, 2004), environmental monitoring (Carrara et al., 2008), natural resources' planning (Malczewski et al., 2003), landslide hazard assessment (Feizizadeh and Blaschke, 2013), earthquake risk assessment (Rashed and Weeks, 2003), water resources management (Chen and Paydar, 2012), geology (de Araújo and Macedo, 2002). In this study, OWA as a spatial MCDA was implemented that allowed us to model thermal comfort for optimistic to pessimistic scenarios. The unique contribution here is that in addition to considering the values and weight of the criteria, the ORness parameter is also reflected, which makes it possible to consider different condition of mind in the model. In previous studies, it was shown that environmental parameters and surface biophysical characteristics such as surface temperature, vegetation cover, built-up lands, surface albedo and solar radiation affect spatio-temporal changes of thermal comfort index measured at

meteorological stations (Van Hove et al., 2015; Qaid et al., 2016; Song and Wu, 2018; Xu et al., 2017; Stathopoulou et al., 2005; Wang et al., 2004; Sobrino et al., 2013; Mahmoud and Gan, 2018). In previous studies, the effect of land surface emissivity as well as SWD to surface were neglected (Mushore et al., 2018; Song and Wu, 2018; Xu et al., 2017; Stathopoulou et al., 2005; Wang et al., 2004; Sobrino et al., 2013; Polydoros and Cartalis, 2014). In this study, by considering LWU instead of LST, the influence of land surface emissivity is also considered in the modeling thermal comfort, because as surface brightness increases, the sensible heat flux increases. This finding suggests that increased brightness can significantly affect the thermal comfort of pedestrians in urban open spaces. Since the thermal comfort depends on the mean radiant temperature, the increase in surface albedo increases the short-wave radiation from the ground to the sky. It should be noted that pedestrians reduce the earth's surface exposed to sun radiation while walking in urban environments, but they suffer both from an increase in the reflected radiation from the surface as well as the direct sun radiation (Taleghani, 2018). The degree of influence for each of the environmental parameters and surface biophysical characteristics on the thermal comfort index is different as shown in Tables 4 and 5. Our results show that based on the correlation coefficient between each of the environmental parameters and surface biophysical characteristics with the values of DI in the geographic location of the meteorological stations, LWU from the surface, SWD to the surface, surface biophysical characteristics of brightness, wetness, greenness and LWD to the surface have the highest impact on the DI, respectively.

Generally, the thermal comfort related to pessimistic circumstances can be useful for sensitive and high-risk groups including the elderly, children and heat sensitive individuals (see Fig. 6). In this case, suitable and very suitable regions were identified. For this reason, the area of these classes in the thermal comfort map is less than the more optimistic condition of mind (see Fig. 7). On the other hand, the output related to the optimistic condition of mind for local individuals who are least sensitive to the thermal conditions of the environment is useful (see Fig. 6). Investigating the results of the spatial MCDA model for Tehran shows that in the cold and warm periods of the year, the western and north-west and the central, northern, and eastern regions respectively, are suitable and very suitable in terms of thermal comfort compared to other regions of the study area. In different conditions of mind, the area and spatial distribution of different classes of thermal comfort are different. In both warm and cold periods of the year with increasing degree of optimism, the area of suitable and the very suitable categories of thermal comfort increase (Fig. 7).

The presented results are sensitive to the following factors: a) the choice of modeling technique and the used thresholds in the model, b) the choice of remote sensing indices e.g., greenness, wetness, brightness, c) heterogeneity of spatial/temporal resolution of satellite images and products. With respect to the latter factor, only a few remote sensing sensors offer the data needed to conduct this study e.g., the thermal images, water vapor products, among others. Future studies should aim at acquiring finer remote sensing data and products with least variability of spatial and temporal resolution of input data.

5. Conclusions

Thermal discomfort has a negative effect on human physical and mental performance causing fatigue, sleep disturbances, reduced ability to perform mental activities, health problems and even death. Therefore, it is of outmost importance to detect, monitor, and predict thermal comfort patterns for solving human health challenge's, improving urban planning practices, optimizing physical sights, climate change adaptation, planning social and economic services, and efficient energy consumption in cities. The heterogeneity across urban environments causes spatial heterogeneity of the thermal comfort of individuals, which are mainly due to environmental and surface conditions. In this study, a GIS-based MCDA model was used for modeling of

thermal comfort of Tehran in different mental circumstances scenarios. The results show that, in different condition of mind, the area and spatial distribution of different classes of thermal comfort are different. Also, with increasing degree of optimism, the area of suitable and unsuitable categories of thermal comfort decreases. The proposed spatial MCDA model can be adapted to model thermal comfort for other cities especially those located in arid regions and are extremely influenced by climate change. As per future directions, the development of a web-based solution for acquiring satellite images (near) real-time and calculating and visualizing the results of thermal comfort is recommended. Furthermore, future studies should incorporate other surface biophysical characteristics such as normalized difference vegetation index (NDVI), temperature vegetation dryness index (TDVI) and soil adjusted vegetation index (SAVI) for modeling thermal comfort (Yuan and Bauer, 2007; Zawadzki et al., 2016).

References

- Allen, R., Tasumi, M., Trezza, R., Waters, R., Bastiaanssen, W. 2002. SEBAL (Surface Energy Balance Algorithms for Land). Advance Training and Users Manual–Idaho Implementation, version, 1, 97.
- Baig, M.H.A., Zhang, L., Shuai, T., Tong, Q., 2014. Derivation of a tasseled cap transformation based on Landsat 8 at-satellite reflectance. *Remote Sens. Lett.* 5, 423–431.
- Bhattacharjee, S., Ghosh, S.K., 2015. SPATIO-temporal change modeling of LULC: a semantic Kriging approach. *ISPRS Ann. Photogramm., Remote Sens. Spatial Inform. Sci.*
- Carlucci, S., Pagliano, L., 2012. A review of indices for the long-term evaluation of the general thermal comfort conditions in buildings. *Energy Build.* 53, 194–205.
- Carrara, P., Bordogna, G., Boschetti, M., Brivio, P.A., Nelson, A., Stroppiana, D., 2008. A flexible multi-source spatial-data fusion system for environmental status assessment at continental scale. *Int. J. Geog. Inf. Sci.* 22, 781–799.
- Chen, Y., Paydar, Z., 2012. Evaluation of potential irrigation expansion using a spatial fuzzy multi-criteria decision framework. *Environ. Model. Software* 38, 147–157.
- Choi, J.-H., Yeom, D., 2019. Development of the data-driven thermal satisfaction prediction model as a function of human physiological responses in a built environment. *Build. Environ.*
- Claus, R., Martin, R., 2004. Personalized multi-criteria decision strategies in location-based decision support. *Geog. Inf. Sci.* 10, 149–156.
- Clements, A.C., Pfeiffer, D.U., Martin, V., 2006. Application of knowledge-driven spatial modelling approaches and uncertainty management to a study of Rift Valley fever in Africa. *Int. J. Health Geographics* 5, 57.
- Cooley, T., Anderson, G., Felde, G., Hoke, M., Ratkowski, A., Chetwynd, J., Gardner, J., Adler-golden, S., Matthew, M., Berk, A., 2002. Flaash, a MODTRAN4-based atmospheric correction algorithm, its application and validation. In: *Geoscience and Remote Sensing Symposium, 2002. IGARSS'02. 2002 IEEE International. IEEE*, pp. 1414–1418.
- De Araújo, C.C., Macedo, A.B., 2002. Multicriteria geologic data analysis for mineral favorability mapping: application to a metal sulphide mineralized area, Ribeira Valley Metallogenic Province, Brazil. *Nat. Resour. Res.* 11, 29–43.
- de Ridder, K., Adamec, V., Bañuelos, A., Bruse, M., Burger, M., Damsgaard, O., Dufek, J., Hirsch, J., Lefebvre, F., Perez-lacorzana, J., 2004. An integrated methodology to assess the benefits of urban green space. *Sci. Total Environ.* 334, 489–497.
- Duffie, J.A., Beckman, W.A., 2013. *Solar Engineering of Thermal Processes*. John Wiley & Sons.
- Feizizadeh, B., Blaschke, T., 2013. GIS-multicriteria decision analysis for landslide susceptibility mapping: comparing three methods for the Urmia lake basin, Iran. *Nat. Hazards* 65, 2105–2128.
- Firozjaei, M.K., Kiavarz, M., Alavipanah, S.K., Lakes, T., Qureshi, S., 2018a. Monitoring and forecasting heat island intensity through multi-temporal image analysis and cellular automata-Markov chain modelling: a case of Babol city, Iran. *Ecol. Indic.* 91, 155–170.
- Firozjaei, M.K., Kiavarz, M., Nematollahi, O., Karimpour Reihan, M., Alavipanah, S.K., 2019. An evaluation of energy balance parameters, and the relations between topographical and biophysical characteristics using the mountainous surface energy balance algorithm for land (SEBAL). *Int. J. Remote Sens.* 1–31.
- Firozjaei, M.K., Nematollahi, O., Mijani, N., Shorabeh, S.N., Firozjaei, H.K., Toomanian, A., 2018b. An integrated GIS-based ordered weighted averaging analysis for solar energy evaluation Iran: current conditions and future planning. *Renewable Energy*.
- García-Herrera, R., Díaz, J., Trigo, R.M., Luterbacher, J., Fischer, E.M., 2010. A review of the European summer heat wave of 2003. *Crit. Rev. Environ. Sci. Technol.* 40, 267–306.
- Geletič, J., Lehnert, M., Savič, S., Milošević, D., 2018. Modelled spatiotemporal variability of outdoor thermal comfort in local climate zones of the city of Brno, Czech Republic. *Sci. Total Environ.* 624, 385–395.
- Gómez, F., Cueva, A.P., Valcuende, M., Matzarakis, A., 2013. Research on ecological design to enhance comfort in open spaces of a city (Valencia, Spain). *Utility of the physiological equivalent temperature (PET)*. *Ecol. Eng.* 57, 27–39.
- Huang, K.-T., Yang, S.-R., Matzarakis, A., Lin, T.-P., 2018. Identifying outdoor thermal risk areas and evaluation of future thermal comfort concerning shading orientation in a traditional settlement. *Sci. Total Environ.* 626, 567–580.
- Jelokhani-Niaraki, M., Malczewski, J., 2015. A group multicriteria spatial decision support system for parking site selection problem: a case study. *Land Use Policy* 42, 492–508.
- Kántor, N., Unger, J., 2010. Benefits and opportunities of adopting GIS in thermal comfort studies in resting places: an urban park as an example. *Landscape Urban Plann.* 98, 36–46.
- Karimi Firozjaei, M., Kiavarz, M., 2018. Investigating the relationship between heat island intensity and biophysical characteristics differences between built-up and non-built-up regions (case study: Cities in East Mazandaran). *J. Geospatial Inf. Technol.* 6, 165–189.
- Karimi Firozjaei, M., Kiavarz Mogaddam, M., Alavipanah, S., Hamzeh, S., 2018. Normalizing satellite images-derived land surface temperature relative to environmental parameters based on the soil and vegetation energy balance equations. *J. Geomatics Sci. Technol.* 7, 213–232.
- Katavoutas, G., Assimakopoulos, M.N., Assimakopoulos, D.N., 2016. On the determination of the thermal comfort conditions of a metropolitan city underground railway. *Sci. Total Environ.* 566, 877–887.
- Kiavarz, M., Jelokhani-Niaraki, M., 2017. Geothermal prospectivity mapping using GIS-based Ordered Weighted Averaging approach: a case study in Japan's Akita and Iwate provinces. *Geothermics* 70, 295–304.
- Li, X., Li, W., Middel, A., Harlan, S., Brazel, A., Turner, B., 2016. Remote sensing of the surface urban heat island and land architecture in Phoenix, Arizona: combined effects of land composition and configuration and cadastral–demographic–economic factors. *Remote Sens. Environ.* 174, 233–243.
- Li, Y., Geng, S., Yuan, Y., Wang, J., Zhang, X., 2018. Evaluation of climatic zones and field study on thermal comfort for underground engineering in China during summer. *Sustainable Cities Soc.* 43, 421–431.
- Liu, L., Lin, Y., Xiao, Y., Xue, P., Shi, L., Chen, X., Liu, J., 2018. Quantitative effects of urban spatial characteristics on outdoor thermal comfort based on the LCZ scheme. *Build. Environ.* 143, 443–460.
- Liu, Q., Liu, G., Huang, C., Liu, S., Zhao, J., 2014. A tasseled cap transformation for Landsat 8 OLI TOA reflectance images. In: *Geoscience and Remote Sensing Symposium (IGARSS), 2014 IEEE International. IEEE*, pp. 541–544.
- Liu, Q., Liu, G., Huang, C., Xie, C., 2015. Comparison of tasseled cap transformations based on the selective bands of Landsat 8 OLI TOA reflectance images. *Int. J. Remote Sens.* 36, 417–441.
- Mahmoud, S.H., Gan, T.Y., 2018. Long-term impact of rapid urbanization on urban climate and human thermal comfort in hot-arid environment. *Build. Environ.*
- Malczewski, J., 2006. Ordered weighted averaging with fuzzy quantifiers: GIS-based multicriteria evaluation for land-use suitability analysis. *Int. J. Appl. Earth Observ. Geoinform.* 8, 270–277.
- Malczewski, J., Chapman, T., Flegel, C., Walters, D., Shrubsole, D., Healy, M.A., 2003. GIS-multicriteria evaluation with ordered weighted averaging (OWA): case study of developing watershed management strategies. *Environ. Plan. A* 35, 1769–1784.
- Malczewski, J., Rinner, C., 2015. *Multicriteria Decision Analysis in Geographic Information Science*. Springer.
- Malik, I.B.I., Dewancker, B.J., 2018. Identification of population growth and distribution, based on urban zone functions. *Sustainability* 10, 930.
- Mirbagheri, B., Alimohammadi, A., 2017. Improving urban cellular automata performance by integrating global and geographically weighted logistic regression models. *Trans. GIS* 21, 1280–1297.
- Moghaddam, M.H.R., Sedighi, A., Fasihi, S., Firozjaei, M.K., 2018. Effect of environmental policies in combating aeolian desertification over Sejzy Plain of Iran. *Aeolian Res.* 35, 19–28.
- Morris, K.I., Chan, A., Morris, K.J.K., Ooi, M.C., Oozeer, M.Y., Abakar, Y.A., Nadzir, M.S.M., Mohammed, I.Y., Al-Qrimli, H.F., 2017. Impact of urbanization level on the interactions of urban area, the urban climate, and human thermal comfort. *Appl. Geogr.* 79, 50–72.
- Mushore, T.D., Odindi, J., Dube, T., Mutanga, O., 2018. Outdoor thermal discomfort analysis in Harare, Zimbabwe in Southern Africa. *South Afr. Geog. J.* 100, 162–179.
- Musse, M.A., Barona, D.A., Rodriguez, L.M.S., 2018. Urban environmental quality assessment using remote sensing and census data. *Int. J. Appl. Earth Obs. Geoinform.* 71, 95–108.
- Panah, S., Mogaddam, M.K., Firozjaei, M.K., 2017. Monitoring spatiotemporal changes of heat island in Babol City due to land use changes. *Int. Arch. Photogramm. Remote Sens. Spatial Inf. Sci.* 42.
- Polydoros, A., Cartalis, C., 2014. Assessing thermal risk in urban areas—an application for the urban agglomeration of Athens. *Adv. Build. Energy Res.* 8, 74–83.
- Qaid, A., Lamit, H.B., Ossen, D.R., Shahminan, R.N.R., 2016. Urban heat island and thermal comfort conditions at micro-climate scale in a tropical planned city. *Energy Build.* 133, 577–595.
- Rashed, T., Weeks, J., 2003. Assessing vulnerability to earthquake hazards through spatial multicriteria analysis of urban areas. *Int. J. Geog. Inf. Sci.* 17, 547–576.
- Santamouris, M., Kolokotsa, D., 2015. On the impact of urban overheating and extreme climatic conditions on housing, energy, comfort and environmental quality of vulnerable population in Europe. *Energy Build.* 98, 125–133.
- Shek, K.W., Chan, W.T., 2008. Combined comfort model of thermal comfort and air quality on buses in Hong Kong. *Sci. Total Environ.* 389, 277–282.
- Sobrino, J.A., Oltra-Carrió, R., Soria, G., Jimenez-Muñoz, J.C., Franch, B., Hidalgo, V., Mattar, C., Julien, Y., Cuenca, J., Romaguera, M., 2013. Evaluation of the surface urban heat island effect in the city of Madrid by thermal remote sensing. *Int. J. Remote Sens.* 34, 3177–3192.
- Song, Y., Wu, C., 2018. Examining human heat stress with remote sensing technology. *GIScience Remote Sens.* 55, 19–37.
- Stathopoulou, M.I., Cartalis, C., Keramitsoglou, I., Santamouris, M., 2005. Thermal remote sensing of Thom's discomfort index (DI): comparison with in-situ measurements. *Remote Sensing for Environmental Monitoring, GIS Applications, and Geology*

- V. International Society for Optics and Photonics 59830K.
- Taleghani, M., 2018. The impact of increasing urban surface albedo on outdoor summer thermal comfort within a university campus. *Urban Climate* 24, 175–184.
- Thom, E.C., 1959. The discomfort index. *Weatherwise* 12, 57–61.
- Toy, S., Yilmaz, S., Yilmaz, H., 2007. Determination of bioclimatic comfort in three different land uses in the city of Erzurum, Turkey. *Build. Environ.* 42, 1315–1318.
- Tsunematsu, N., Yokoyama, H., Honjo, T., Ichihashi, A., Ando, H., Shigyo, N., 2016. Relationship between land use variations and spatiotemporal changes in amounts of thermal infrared energy emitted from urban surfaces in downtown Tokyo on hot summer days. *Urban Climate* 17, 67–79.
- United Nations 2018. *World Urbanization Prospects: The 2018 Revision*.
- van Hove, L., Jacobs, C., Heusinkveld, B., Elbers, J., van Driel, B., Holtslag, A., 2015. Temporal and spatial variability of urban heat island and thermal comfort within the Rotterdam agglomeration. *Build. Environ.* 83, 91–103.
- Wang, J., Meng, Q., Tan, K., Zhang, L., Zhang, Y., 2018a. Experimental investigation on the influence of evaporative cooling of permeable pavements on outdoor thermal environment. *Build. Environ.* 140, 184–193.
- Wang, W., Zhu, L., Wang, R., 2004. An analysis on spatial variation of urban human thermal comfort in Hangzhou, China. *J. Environ. Sci. (China)* 16, 332–338.
- Wang, Y., Ni, Z., Peng, Y., Xia, B., 2018b. Local variation of outdoor thermal comfort in different urban green spaces in Guangzhou, a subtropical city in South China. *Urban Forestry Urban Green.* 32, 99–112.
- Waters, R., Allen, R., Bastiaanssen, W., Tasumi, M., Trezza, R. 2002. *SEBAL. Surface Energy Balance Algorithms for Land. Idaho Implementation. Advanced Training and Users Manual, Idaho, USA*.
- Weng, Q., Firozjaei, M.K., Kiavarz, M., Alavipanah, S.K., Hamzeh, S., 2019. Normalizing land surface temperature for environmental parameters in mountainous and urban areas of a cold semi-arid climate. *Sci. Total Environ.* 650, 515–529.
- Weng, Q., Firozjaei, M.K., Sedighi, A., Kiavarz, M., Alavipanah, S.K., 2018. Statistical analysis of surface urban heat island intensity variations: a case study of Babol city, Iran. *GISci. Remote Sens.* 1–29.
- WORLDPOPULATIONREVIEW 2018. <http://worldpopulationreview.com>.
- Xu, H., Hu, X., Guan, H., He, G., 2017. Development of a fine-scale discomfort index map and its application in measuring living environments using remotely-sensed thermal infrared imagery. *Energy Build.* 150, 598–607.
- Xu, Z., Etzel, R.A., Su, H., Huang, C., Guo, Y., Tong, S., 2012. Impact of ambient temperature on children's health: a systematic review. *Environ. Res.* 117, 120–131.
- Yager, R.R., 1988. On ordered weighted averaging aggregation operators in multicriteria decisionmaking. *IEEE Trans. Systems Man Cybernetics* 18, 183–190.
- Yan, H., Wu, F., Dong, L., 2018. Influence of a large urban park on the local urban thermal environment. *Sci. Total Environ.* 622, 882–891.
- Yuan, F., Bauer, M.E., 2007. Comparison of impervious surface area and normalized difference vegetation index as indicators of surface urban heat island effects in Landsat imagery. *Remote Sens. Environ.* 106, 375–386.
- Zawadzki, J., Cieszewski, C.J., Zasada, M., Lowe, R.C., 2005. Applying geostatistics for investigations of forest ecosystems using remote sensing imagery. *Silva Fennica* 39, 599.
- Zawadzki, J., Przeździecki, K., Miatkowski, Z., 2016. Determining the area of influence of depression cone in the vicinity of lignite mine by means of triangle method and LANDSAT TM/ETM+ satellite images. *J. Environ. Manage.* 166, 605–614.
- Zhang, Y., Odeh, I.O., Han, C., 2009. Bi-temporal characterization of land surface temperature in relation to impervious surface area, NDVI and NDBI, using a sub-pixel image analysis. *Int. J. Appl. Earth Observ. Geoinform.* 11, 256–264.
- Zhu, H., Wang, H., Liu, Z., Li, D., Kou, G., Li, C., 2018. Experimental study on the human thermal comfort based on the heart rate variability (HRV) analysis under different environments. *Sci. Total Environ.* 616, 1124–1133.